Transient Experimental Investigation of Micro Heat Pipes

D. Wu* and G. P. Peterson†
Texas A&M University, College Station, Texas 77843
and
W. S. Chang‡
Wright Research and Development Center, Wright-Patterson Air Force Base, Ohio 45433

An experimental investigation was conducted on several small, tapered micro heat pipes specifically designed for use in the thermal control of ceramic chip carriers to verify the operation, measure the performance limits and transient behavior, and determine the accuracy of a previously developed numerical model. Several heat pipes were evaluated for transient conditions, i.e., startup or rapid changes in the thermal load. The experimental data are compared with the results of a previously developed analytical model to determine the accuracy of the model and verify the predicted trends. The experimental results indicated that the transient numerical model is capable of accurately predicting the maximum transport capacity prior to the onset of dry out, the temperature distribution throughout the longitudinal position, and the temperature difference between axial locations on the heat pipe to within 0.3°C. Although the numerical model was found to accurately predict the steady-state behavior, the numerical model substantially underestimated the transient response.

Nomenclature

A = cross-sectional area
C_p = specific heat
Q = heat transfer
r = radius of curvature
T = temperature
ρ = density

Subscripts
c = capillary, curvature
h = hydraulic
l = liquid
s = solid
v = vapor, viscous

Introduction

As noted in several recent reviews,[1,2] the need to develop microelectronic devices capable of operating at increased performance levels with high reliability requires better methods of thermal control. As miniaturization and component density increase, the thermal management problem will continue to grow in both significance and complexity. This will require innovative cooling methods by which heat from localized heat sources can be transferred to alternate locations where it can be dissipated. One proposed method for accomplishing this is to utilize micro heat pipes. By locating the evaporator adjacent to the heat source and a finned condenser some distance away, heat can be removed and dissipated by either free or forced convection, as illustrated in Fig. 1.

Babin et al.[3] described a micro heat pipe as one which satisfies the condition

$$\frac{r_c}{r_h} > 1 \tag{1}$$

where r_c is the capillary radius of the heat pipe and r_h is the hydraulic radius of the flow channel. In micro heat pipes as in more conventional ones, the high thermal conductivity is the result of the vaporization and condensation process occurring in the evaporator and condenser, respectively.[4,5] For this reason, determination of the evaporation and condensation rate of the liquid plays a key role in evaluating the thermal characteristics and heat transport limitations of these heat pipes.[6]

Micro heat pipes have a wide range of applications including the thermal control of discrete semiconductor devices or infrared detectors and the heat removal from the leading edges of hypersonic aircraft.[7] Smaller micro heat pipes (less than 0.05 mm² in cross-sectional area) could be incorporated into semiconductor devices as an integral part of the chip.[8] This would provide a mechanism for eliminating the localized hot spots associated with semiconductor devices and significantly improve the chip reliability. In addition, these micro heat pipes could provide a method for collecting and dissipating the high thermal loads associated with the three-dimensional chip architectures being developed for use in fifth generation computers.[9]

Because of the wide range of potential applications for these devices, micro heat pipes have been the subject of several investigations. The first of these focused on the steady-state modeling and testing of a trapezoidal micro heat pipe approximately 1 mm² in cross-sectional area and 57 mm in length.[3] The second involved the development of a numerical model designed to predict the transient behavior during startup and/or the behavior during rapid changes in the operating power level.[10] Although the two previously developed models have both been shown to predict the steady-state performance limitations and operational characteristics with a reasonable degree of accuracy, no transient experimental data have been obtained and little is known about the accuracy of these two models during startup or rapid changes in the evaporator thermal load. For this reason, an investigation was conducted to obtain experimental data for comparison with this transient numerical model.

Using the information from these two models, several test articles were designed and constructed. These test articles had

Presented as Paper 90-1791 at the AIAA/ASME Joint Heat Transfer Conference, Seattle, WA, June 18–20, 1990; received April 27, 1990; revision received Oct. 30, 1990; accepted for publication Nov. 21, 1990.

*Research Associate, Mechanical Engineering Department.
†Professor of Mechanical Engineering. Associate Fellow AIAA.
‡Research Scientist. Member AIAA.

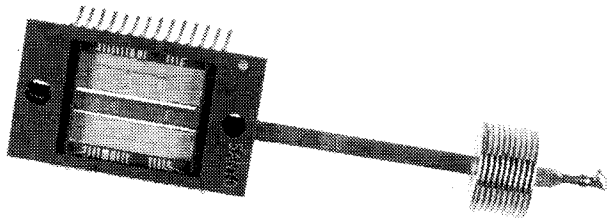

Fig. 1 Tapered micro heat pipe application.

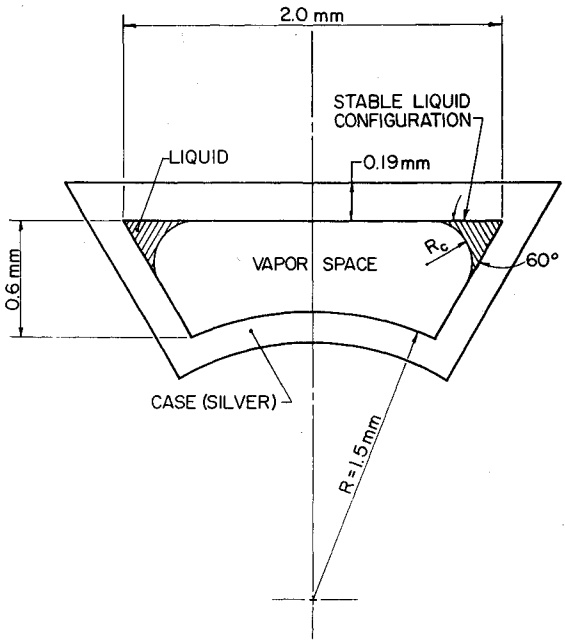

Fig. 2 Cross-sectional shape of the modeled heat pipe.

outer dimensions of approximately 1 mm by 2 mm as shown in Fig. 2, and approximately 60 mm in length. The test articles were constructed from silver and charged with 0.032 g of ultrapure deionized water. In addition to several charged test articles, an uncharged test pipe was evaluated to establish a baseline value from which the improvement in the heat transport capacity due to the vaporization and condensation could be determined.

Numerical Model

The numerical model used in this investigation was originally developed as a design tool for helping to better understand the effects of variations in the geometry, the liquid-solid wetting angle, the amount of working fluid, and continued size reductions. A detailed description of the model, the grid independence, and the predicted results have been previously published[10] and indicate that the vaporization and condensation rates within micro heat pipes are extremely sensitive to changes in the vapor pressure. For this reason, the numerical model initially assumed that the vaporization and condensation rates were directly proportional to the liquid-vapor interface area for a given element and a predictor-corrector treatment was applied to obtain a stable solution. In this process, the evaporation rate was initially assumed to be equal to the condensation rate and the resulting vapor pressure was calculated. This vapor pressure was then used to compute the change in the mass of vapor and, hence, the difference between vaporization and condensation. The original assumption of equal vaporization and condensation rates was then checked and the values updated. Preliminary tests indicated that the solution was stable regardless of the time step used.

The energy equation used in the transient model was written as

$$\dot{Q}_{\text{in}} = \dot{Q}_{\text{out}} + \dot{Q}_r \tag{2}$$

where

$$Q_r = \int \rho_l A_l C_{pl} \frac{dT_l}{dx}\,dx + \int \rho_v A_v C_{pv} \frac{dT_v}{dx}\,dx + \int \rho_s A_s C_{ps} \frac{dT_s}{dx}\,dx \tag{3}$$

C_{pl}, C_{pv}, and C_{ps} are the heat capacities of the liquid, vapor, and solid boundaries, respectively, and the ΔT's are the corresponding temperature changes.

The continuity equation was written as

$$\int \rho_v A_v dx + \int \rho_l A_l dx = \text{Fluid charge} \tag{4}$$

and the total volume inside the heat pipe was defined and expressed as

$$Vol_{\text{Total}} = Vol_l + Vol_v \tag{5}$$

and

$$A = A_l + A_v, \tag{6}$$

respectively.[10]

As is the case for larger heat pipes, micro heat pipes consist of three basic sections: an evaporator, a condenser, and an adiabatic section that separates evaporator and condenser. Each of these sections has a different set of boundary conditions and as a result was treated independently. The single boundary condition utilized in the evaporator section was the time-dependent heat flux. For a specific input heat flux, the saturation pressure at a given location was obtained by using a combination of the molecular flux and the energy conservation equation. In the adiabatic section, the latent heat absorbed by evaporation and given up by condensation was assumed to be equal to the sensible heat absorbed or rejected by the liquid and/or the heat pipe case. In the condenser region, the boundary temperature of the heat pipe was assumed to be constant, resulting in governing equations similar to those used in the adiabatic section. Although in normal operation, the condenser boundary temperature would vary with the input power, in a controlled laboratory experiment constant condenser temperatures are easily obtained by controlling the temperature and/or flowrate of the circulating coolant.

The transient numerical model indicated that the vapor temperature variations were proportional to the heat input and that without dry out or flooding, the effective conductivity of the heat pipe was independent of time shortly after startup. In contrast, a fairly long period of time was required for the other thermal parameters to reach their steady-state values. For example, the time required for the outer case to reach steady state ranged from 30 to 80 s after full heat input, and was found to be dependent on the wetting angle. The smaller the wetting angle and the higher the temperature, the shorter the time required.

The most interesting result of the numerical modeling effort was the behavior of the liquid in the corner regions. As shown in Fig. 3, the numerical model predicted reverse liquid flow during startup. Although not well understood, it was hypothesized that this reverse liquid flow was the result of an imbalance in the overall pressure drop, i.e., because the evap-

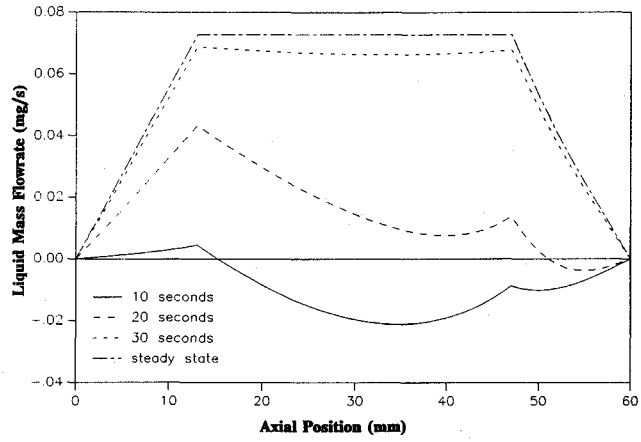

Fig. 3 Liquid mass flow rate as a function of time and axial position.

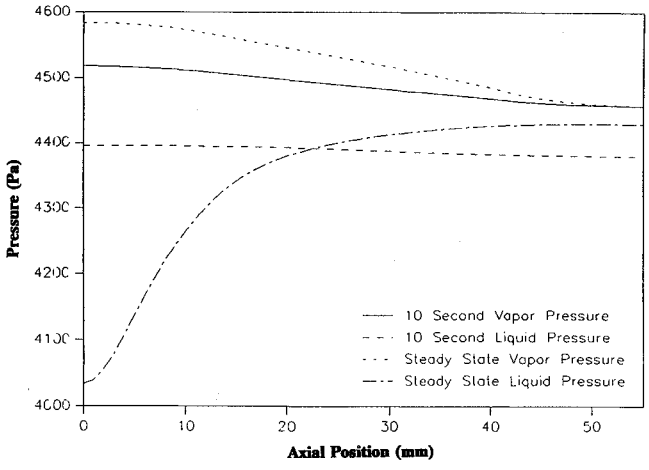

Fig. 4 Liquid and vapor pressure as a function of axial position.

oration rate does not provide a sufficient change in the liquid-vapor interfacial curvature adequate to compensate for the total pressure drop resulting from the temperature change. Some liquid is forced from the evaporator region towards the condenser region through the corners of the heat pipe. Once the heat pipe reaches full power, the reverse liquid flow disappears and the liquid mass flow rate gradually increases until a steady-state condition is reached and the liquid mass flow rate is equal to the vapor mass flow rate in any given section. This phenomena is more apparent in Fig. 4, which illustrates the pressure as a function of axial position 10 s after startup and at steady-state. As illustrated, shortly after startup the pressure of both the liquid and vapor are higher in the evaporator than in the condenser and gradually decrease with position. This is the phenomena which promotes flow away from the evaporator and towards the condenser. Once steady state has been achieved, the liquid pressure is much lower in the evaporator region and increases dramatically with position, promoting flow back towards the evaporator.

Experimental Program

To verify the accuracy of the transient model and determine the maximum heat transport capacity, experimental investigations were conducted using a tapered micro heat pipe designed specifically for use in the thermal control of ceramic chip carriers. In the application illustrated in Fig. 1, this micro heat pipe fits securely under the chip and is attached to the chip carrier. Small fins located at the condenser end of the heat pipe promote the cooling of the condenser by free convection.

Test Facility

The experimental test facility used for this investigation has been previously described by Peterson, et al.[7] and consisted of five subsystems: the test stand, a variable heat source, a constant temperature circulating bath, a data acquisition system, and a vacuum system. The test stand was constructed from Plexiglas and provided a means for rotating the test pipes through an angle of 360 deg. In this way, tests could be conducted at tilt angles which both helped and hindered the return of liquid back to the evaporator. The test stand also supported an aluminum cooling chamber, which surrounded the condenser region of the heat pipe. A circulating bath provided a constant temperature ethyl-glycol solution to the cooling chamber where it flowed over the condenser portion of the heat pipe at a constant rate of approximately seven liters per minute. Heat was supplied to the evaporator portion of the heat pipe by a thin nichrome strip heater cemented to the top portion of the heat pipe. The power was monitored by measuring the voltage and current to the heater.

Two separate techniques were used to monitor the temperature distribution of the heat pipe. The first of these consisted of a series of eight Special Limit of Error (SLE) Copper-Constantan (AWG 36) thermocouples with a measurement uncertainty of ± 0.5°C. Three thermocouples were attached to the underside of the heat pipe at equidistant positions on the evaporator; four in the adiabatic region, and one at the inlet to the cooling chamber, as shown in Fig. 5. The second technique used to monitor the temperature distribution was an infrared thermal measurement system. A Hughes Probe Eye TVS Model 3000 Infrared Camera in conjunction with an RGB monitor and a real time recorder were used to observe the temperature profile of the test pipe during both startup and steady-state operation. Using this system, the temperature variation along the heat pipe could be measured with a resolution of approximately ± 0.05°C. It is important to note that the measurements of interest in this investigation were temperature differences not absolute temperatures. For this reason special care was taken to insure that the temperature measurement techniques were extremely repeatable (i.e., two thermocouples at the same temperature resulted in the same value) even if the absolute value was not totally accurate. In this way, small temperature differences could be measured with greater accuracy.

To reduce any heat losses through convection, the tests were conducted in a vacuum of less than 10^{-2} Torr. The entire test facility was encased in a stainless-steel vacuum chamber equipped with a single crystal silicon window, as shown in Fig. 6, to allow observation with the thermal measurement system. A mechanical roughing pump in series with an oil diffusion pump was used to obtain the required vacuum.

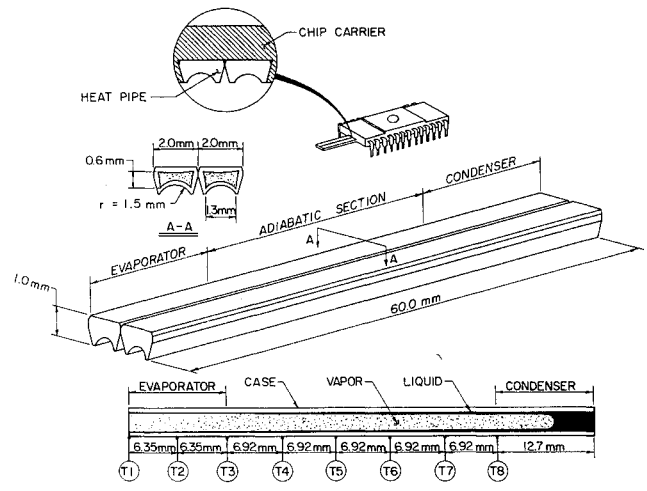

Fig. 5 Location of thermocouples.

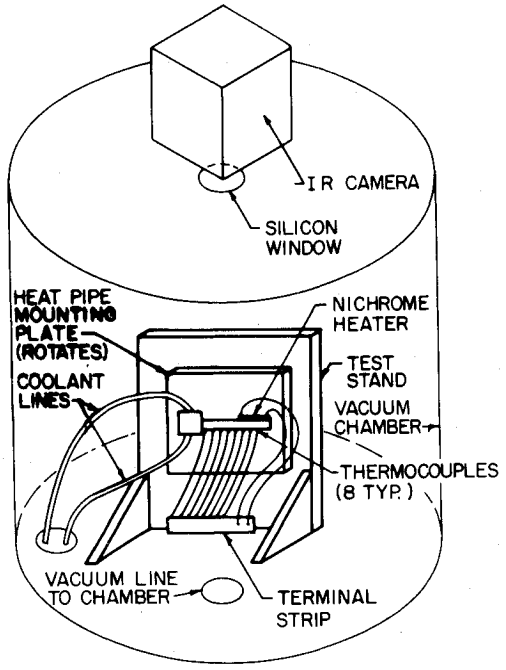

Fig. 6 Experimental test facility.

Experimental Procedure

In order to fully understand the operational characteristics and performance limitations of this tapered micro heat pipe, an experimental test plan was developed. This test plan was comprised of three principal tasks: 1) testing of a charged silver heat pipe to determine the transient characteristics; 2) testing of a charged silver heat pipe to determine the steady-state behavior for different temperatures and tilt angles; and 3) testing of an uncharged silver heat pipe for comparison with the charged heat pipe results.

The heat pipe was first instrumented with the thermocouples and then the nichrome resistance heater was attached to the upper surface of the evaporator. All of the data reported here were for condenser and evaporators 1.27 cm in length with the remaining portion serving as the adiabatic region. After all surfaces had been painted with a flat black paint of known emissivity to enhance the IR resolution, the entire assembly was mounted on the test fixture and loaded into the vacuum chamber. Once the desired vacuum had been obtained, the cooling bath temperature was adjusted and the power to the evaporator portion of the heat pipe was turned on and thermocouple measurements were taken at approximately 0.5-s intervals with temperature readings for each of the eight thermocouples recorded as a function of time.

The heat input for the steady-state tests was increased in small increments until the desired operating temperature had been reached. Preliminary tests indicated that a time of approximately 20 min. was necessary for the heat pipe, cooling chamber, and heat spreader to reach steady state. Once steady-state conditions had been achieved, the temperature data as measured by both the infrared camera and the thermocouples were recorded along with the time, date, power level, temperatures, and coolant bath temperature. To obtain data for the next successive power level, the heat flux was incremented and the temperature of the coolant bath adjusted in order to maintain a constant vapor temperature as measured by the thermocouple attached to the outer surface of the adiabatic section. This procedure was followed until the conductance of the heat pipe, defined as the measured input power divided by the measured temperature difference between the evaporator and the condenser sections, approached a constant value and was then repeated for each new operating temperature.

Results and Discussion

Figure 7 illustrates the transient temperature characteristics of the tapered micro heat pipe for an input power of 0.508 W and a condenser temperature of 23°C. The ordinate is shown as a temperature difference between the thermocouple located at the inlet to the condenser and the one indicated in the legend. As illustrated, the heat pipe reaches a steady-state value very quickly with approximately 90% of the maximum temperature obtained in approximately 20 s. At a time of less than 20 s Thermocouples 1 and 3 yield approximately identical readings. At 15 s, however, they begin to separate and the temperatures start to diverge. This rapid separation is believed to be the result of the onset of dry out. It should be noted that both Thermocouples 1 and 3 are considerably hotter than Thermocouple 2. This may be due to the presence of the lead wires at each end of the heater, but this has not been verified. In situations where there is no dry out in the evaporator, the temperature differences between Thermocouples 1 and 2, and 2 and 3, respectively, would be approximately equal.

Figure 8 illustrates the temperature difference between each of the thermocouples as a function of the power input. Again the abscissa is shown as a temperature difference between the thermocouple located at the inlet to the condenser and the one indicated in the legend. As illustrated, the heat pipe remains approximately isothermal along the entire length for powers between approximately 0.5 and 1.3 W. Prior to the power level of 0.5 W, a majority of the heat is either conducted axially through the wall of the heat pipe or radiated to the environment. At a value of 1.3 W, rapid increases in the evaporator temperature (as indicated by Thermocouples 1,

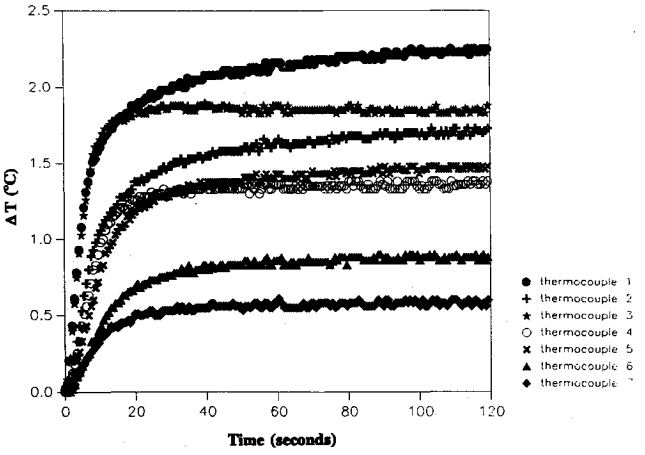

Fig. 7 Transient temperature distribution (Power = 0.058 W, T_c = 23°C).

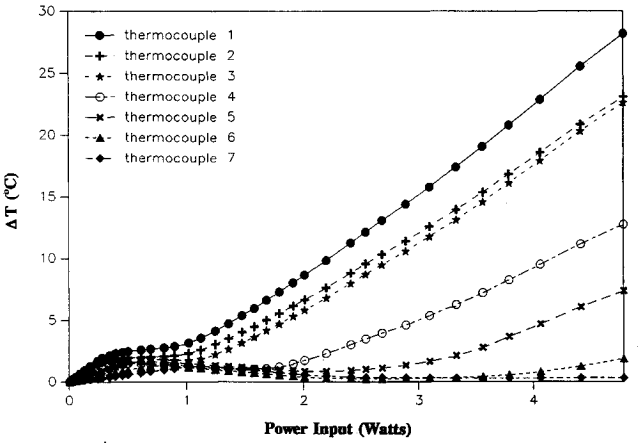

Fig. 8 Steady-state temperature distribution as a function of the input power (No tilt, T_c = 24.5°C).

2, and 3) occur. These increases cascade throughout the evaporator which indicate that dryout has begun and is progressing along the length. This is more apparent in Fig. 9, which illustrates the same experimental results with the axis enlarged to clarify the temperature differences. At approximately 2 W, this dry out has reached Thermocouple 4 located in the adiabatic section. This dry out "front" then proceeds reaching Thermocouple 5 at a power of approximately 3 W. It is interesting to note that at approximately 0.4 W Thermocouples 3 and 4 invert as do Thermocouples 6 and 7 at a power of approximately 0.9 W. No explanation has been developed to determine the cause of this phenomena, however, it was shown to be repeatable.

As mentioned previously, at power levels below 0.5 W, much of the heat is given off by radiation or conducted axially through the wall of the heat pipe. This is more clearly apparent in Fig. 10, which illustrates the experimental results for an uncharged heat pipe using the same condenser temperature and power levels used for the previous figures. As illustrated, the temperature difference indicated by the straight line, has the same slope for each of the corresponding thermocouples indicating that at these power levels, the axial temperature drop is the same for both the uncharged and charged heat pipes. However, as the power level increases, the heat pipe begins to operate more efficiently and the axial temperature drop remains constant. This phenomena is similar to that observed in very short heat pipes. At low powers they are relatively inefficient due to the thermal resistance of the case, wick, etc., but as the length increases the advantages become more apparent.[11]

Comparison of Experimental and Analytical Results

Figure 11 compares the steady-state experimental results obtained in this investigation with the results of the transient model (at steady state) as a function of the operating temperature. As shown, the results compare quite favorably with the largest error occurring at the lower operating temperatures. Figure 12 compares the experimentally measured temperature distribution (again at steady state) with the distribution predicted by the numerical model for a power level of 0.12 W. As illustrated, the temperature data closely follow the predicted trend. Some heat rejection occurs in the adiabatic section, however, the condenser temperature remains relatively constant. Throughout the entire length the predicted and measured temperature distributions are extremely close to the predicted value, with the largest deviation being less than 0.3°C.

In order to determine the effect of tilt angle on the operation of the tapered micro heat pipe, several tests were conducted with similar input powers, but at different tilt angles. Figure 13 compares the predicted and the measured temperature difference between the evaporator, Thermocouple 1, and the condenser, Thermocouple 9, as a function of time for a power input of 0.12 W at a horizontal position. As illustrated, the final steady-state temperature difference between the evaporator and the condenser as predicted by the model is within 12% of the measured value. The numerical model, however, predicts a much more rapid startup of the heat pipe than that obtained experimentally. This predicted rapid startup may be the result of the inherent shortcomings of the model, which assumes that heat is rejected from the evaporator portion of the heat pipe through vaporization of the

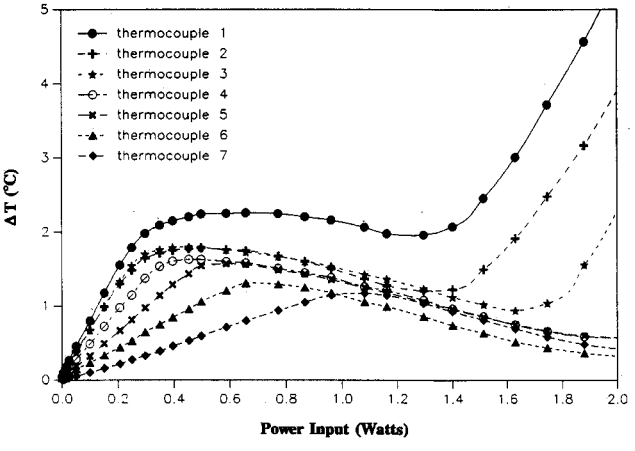

Fig. 9 Enlarged steady-state temperature distribution as a function of the input power (No tilt, T_c = 24.5°C).

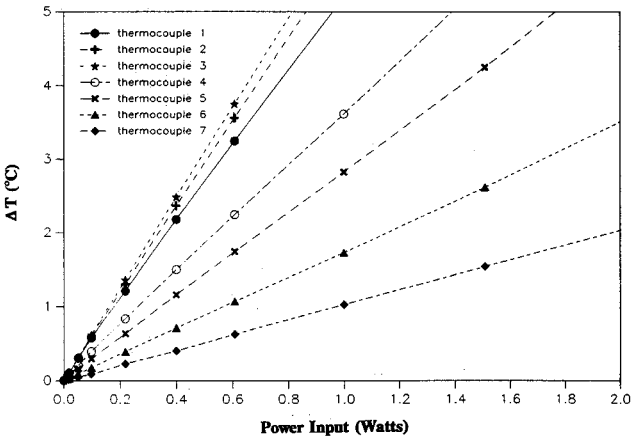

Fig. 10 Steady-state temperature distribution as a function of the input power for an uncharged heat pipe, T_c = 24.5°C.

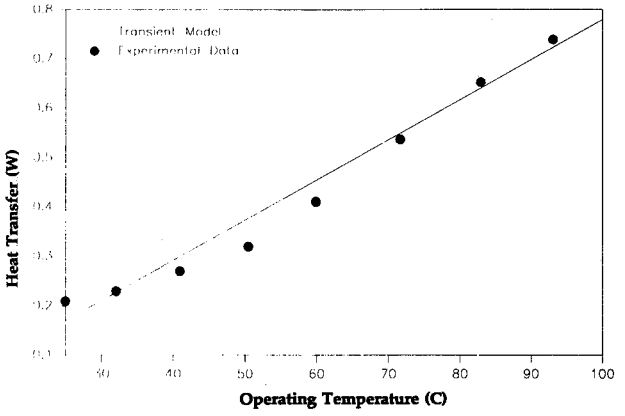

Fig. 11 Comparison of the predicted and experimental maximum transport capacity for steady-state operation as a function of operating temperature.

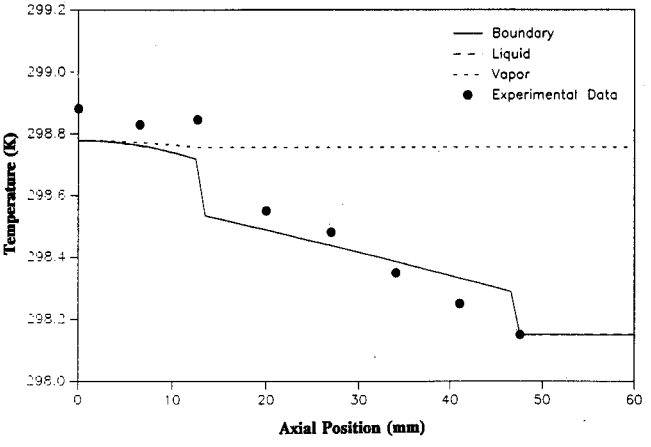

Fig. 12 Steady-state comparison of predicted and measured boundary temperature distribution, (Power = 0.12 W, T_c = 24.5°C, no tilt).

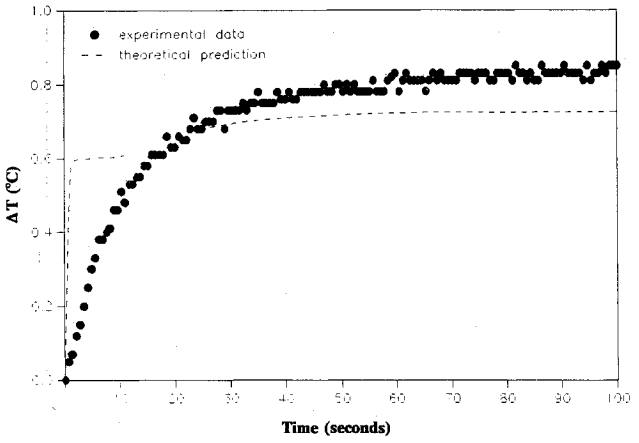

Fig. 13 Comparison of predicted and measured evaporator temperature difference as a function of time, (Power = 0.12 W, T_c = 24.5°C, evaporator down).

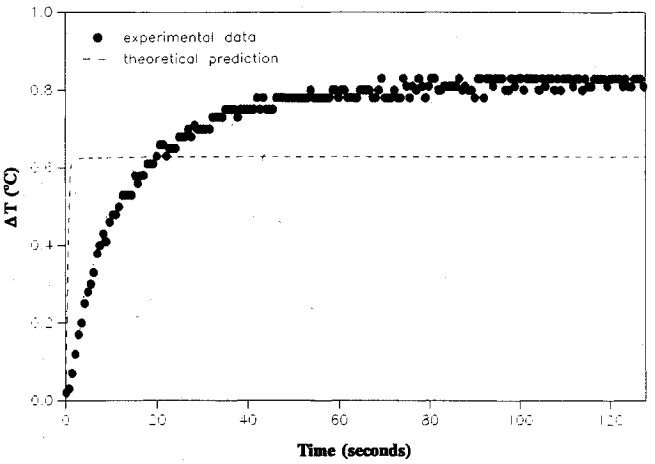

Fig. 14 Comparison of predicted and measured evaporator temperature difference as a function of time, (Power = 0.12 W, T_c = 24.5°C, no tilt).

liquid. In the actual case, it is also rejected through conduction to the support member and radiation to the surroundings. In addition, the numerical model assumes instantaneous heat addition. In the experimental case, some sensible heat is absorbed by the mass of the heater wires, the heater, and the lead wires. The small dip in the predicted temperature difference occurring at approximately 10 s into the test is believed to be the result of the reverse liquid flow discussed previously. As shown, the experimental results indicate no such reverse flow. This may be due to the reduced time constant caused by the mass of heat pipe case material.

Figure 14 illustrates a similar comparison at a tilt angle of 15 deg (evaporator down). As shown, for this case, the numerical model does not predict any reverse liquid flow and significantly underestimates the longitudinal temperature difference. Again, the disparity between the measured and predicted values is believed to be due to differences in the numerical model and the actual experimental tests. In the numerical model the effects of the end wall of the heat pipe were not incorporated. This end region provides an additional capillary radius which helps retain liquid in the evaporator and results in higher power levels prior to the onset of dry out. These increased power levels manifest themselves as an increase in temperature differences, similar to that shown in Fig. 14.

Conclusion

An investigation was conducted to provide information on the transient performance of a tapered micro heat pipe for comparison with a previously developed numerical model. Several heat pipes were evaluated experimentally to determine their suitability for heat removal from a ceramic chip carrier and to provide data with which a previously developed numerical model could be validated. The experimental results indicated that the transient numerical model is capable of accurately predicting the maximum steady-state transport capacity prior to the onset of dryout, the steady-state temperature distribution as a function of the longitudinal position, and the steady-state temperature difference between axial locations on the heat pipe to within 0.3°C prior to the onset of dryout. Although the previously developed numerical model accurately predicted the steady-state behavior, the numerical model substantially underestimated the transient response as measured in this investigation.

As a result of this effort, the numerical model can be used to predict the steady-state behavior and to identify, evaluate, and better understand the phenomena that govern the transient behavior of micro heat pipes as a function of the physical shape, properties of the working fluid, and principal dimensions.

Acknowledgment

The authors would like to acknowledge the support of the TAMU Center for Commercialization of Space Power, Wright Research and Development Center, Itoh Research and Development Corporation of Japan, the Texas Higher Education Coordinating Board (ATP), and the Houston Area Research Center.

References

[1]Marto, P. J., and Peterson, G. P., "Application of Heat Pipes to Electronics Cooling," *Advances in Thermal Modeling of Electronic Components and Systems*, A. Bar-Cohen and A. D. Kraus (editors), Hemisphere Publishing Corporation, New York, 1988, pp. 283–336.

[2]Peterson, G. P., and Ortega, A., "Thermal Control of Electronic Equipment and Devices," *Advances in Heat Transfer*, J. P. Hartnett and T. F. Irvine (editors), Academic Press, New York, 1990, pp. 181–299.

[3]Babin, B. R., Peterson, G. P., and Wu, D., "Analysis and Testing of a Micro Heat Pipe During Steady-State Operation," ASME National Heat Transfer Conference, ASME Paper No. 89-HT-18, Philadelphia, PA, Aug. 6–9, 1989.

[4]Chi, S. W., *Heat Pipe Theory and Practice*, McGraw-Hill Publishing Company, New York, 1976.

[5]Dunn, P. D., and Reay, D. A., *Heat Pipes*, 3rd edition, Pergamon Press, New York, 1982.

[6]Colwell, G. T., and Chang, W. S., "Measurements of the Transient Behavior of a Capillary Structure Under Heavy Thermal Loading," *International Journal of Heat and Mass Transfer*, Vol. 27, No. 4, 1984, pp. 541–551.

[7]Babin, B. R., Peterson, G. P., and Wu, D., "Steady-state Modeling and Testing of a Micro Heat Pipe, *ASME Journal of Heat Transfer*, Vol. 112, No. 3, 1990, pp. 595–601.

[8]Weichold, M. H., Peterson, G. P., and Mallik, A., U.S. Patent Pending, Patent Application #380,189, U.S. Patent and Trademark Office, Filed on July 14, 1989.

[9]Peterson, G. P., "Heat Removal Key to Shrinking Avionics," *Aerospace America*, Vol. 25, No. 8, 1987, pp. 20–22.

[10]Wu, D., and Peterson, G. P., "Investigation of the Transient Characteristics of a Micro Heat Pipe," *AIAA Journal of Thermophysics and Heat Transfer*, Vol. 4, No. 4, 1990.

[11]Babin, B. R., and Peterson, G. P., "Experimental Investigation of a Flexible Bellows Heat Pipe for Cooling Discrete Heat Sources," *ASME Journal of Heat Transfer*, Vol. 112, No. 3, 1990, pp. 602–607.